Journal of Asian Earth Sciences: X 4 (2020) 100034

Contents lists available at ScienceDirect

Journal of Asian Earth Sciences: X

journal homepage: www.journals.elsevier.com/journal-of-asian-earth-sciences-x

Evidence of an east-dipping slab beneath the southern end of the Philippine Trench (1°N–6°N) as revealed by ISC-EHB

Po-Fei Chen[a,*], Mei Chien[a], Craig R. Bina[b], Hung-Yu Yen[a], Erlinton Antonio Olavere[c]

[a] Department of Earth Sciences, National Central University, Taoyuan, Taiwan
[b] Department of Earth and Planetary Sciences, Northwestern University, Evanston, IL, USA
[c] Department of Science and Technology - Philippine Institute of Volcanology and Seismology, Philippines

ARTICLE INFO

Keywords:
Mindanao-Molucca region
Divergent double subduction
East-dipping slab beneath Philippine Trench
Subduction polarity flip
Halmahera slab

ABSTRACT

We examine recently released global seismic datasets in 3D visualization to study slab configurations in the Mindanao-Molucca region, where the present-day arc-arc collision of divergent double subduction propagates northward and attains completion on Mindanao Island, Philippines. The activity of inter-plate thrust earthquakes in the Philippine Trench is not significant until Mindanao (6°N) is reached, while shallow earthquakes on the island exhibit predominantly strike-slip movements on the Cotabato and Philippine Faults. The spatial distributions of GCMT thrust-type earthquakes shallower than 60 km reveal that current collisions mostly occur along the Central and Talaud-Miangas Ridges. ISC-EHB events deeper than 80 km, as well as Slab2 contours, show the eastward-dipping trench of the Halmahera slab flipping to the westward-dipping Philippine Trench northward. We identify a zone of ISC-EHB earthquakes steeply dipping to the east beneath the southern end of the Philippine Trench (1°N–6°N) that is not modeled by Slab2. This feature of a steeply east-dipping slab is explained by collision of the subduction arc and is consistent with steeply plunging **T**-axes of earthquakes. The identification of the east-dipping slab and estimation of its extent are crucial for understanding geodynamic and plate-boundary evolution in the Mindanao-Molucca region.

1. Introduction

The Mindanao-Molucca region is located at the complex junction of the Eurasian, India-Australian, Pacific, and Philippine Sea plates (Fig. 1; please refer to geographic and terrane locations in Fig. 1 hereafter). The geodynamic evolution of this region can be represented using northward distance as a proxy for time-progression of collision. The Molucca Sea (2°S-3°N) to the south is the only present-day arc-arc collision of divergent double subduction (Soesoo et al., 1997), as manifested by inverted-U-shaped Wadati-Benioff zones in the upper mantle. Here, the NW convergence rates (~9 cm/yr; Seno et al., 1993) between the Eurasia and Philippine Sea plates were mostly accommodated by collision of the Sangihe Arc to the west and the Halmahera Arc to the east. To the north, Mindanao Island is attributed to the completion of collision with the Pliocene-Pleistocene accretion of Philippine Sea Plate fragments against the Eurasian Margin, as documented (Quebral et al., 1996), and with initiation of the Philippine and Cotabato Trenches. The Mindanao-Molucca region thus provides a natural laboratory to study the evolution of arc-arc collision, followed by subduction renewal.

On the west margin of the Molucca Sea, the Sangihe slab exhibits profiles of continuous Wadati-Benioff zones on top of positive *P*-wave velocity anomalies (Fig. 2) laterally extending from north Sulawesi to West Mindanao (Amaru, 2007; Hall and Spakman, 2015). On the east margin of the Molucca Sea, however, the seismicity patterns are complex and the positive *P*-wave anomalies are less conspicuous (Fig. 2), coupled with discontinuous and dislocated ridge features – Halmahera Arc, Snellius Ridge, Talaud-East Mindanao. As a result, the relationships between the east-dipping Halmahera slab to the south and the west-dipping Philippine slab to the north remain unresolved. Various plate boundaries in this area have been proposed (Nichols et al., 1988). Based on earthquake observations, Cardwell et al. (1980) suggested the presence of a transform fault connecting the southern end of the Talaud-East Mindanao Ridge easterly to the Ayu Trough near 133°E, and McCaffrey (1982) suggested that a transform fault passes through or close to Morotai but stops at the Philippine Trench. Studies of gravity, magnetics, and seismic reflections, on the other hand, tend to conclude that the Snellius Ridge was a northern extension of the Halmahera Arc and the Philippine Trench south of 6°N was a recently developed feature without connection to another plate boundary (Moore and Silver, 1983; Lallemand et al., 1998; Pubellier et al., 1999). However, high-

* Corresponding author.
E-mail address: bob@ncu.edu.tw (P.-F. Chen).

https://doi.org/10.1016/j.jaesx.2020.100034
Received 25 May 2020; Received in revised form 17 August 2020; Accepted 27 September 2020
Available online 17 October 2020

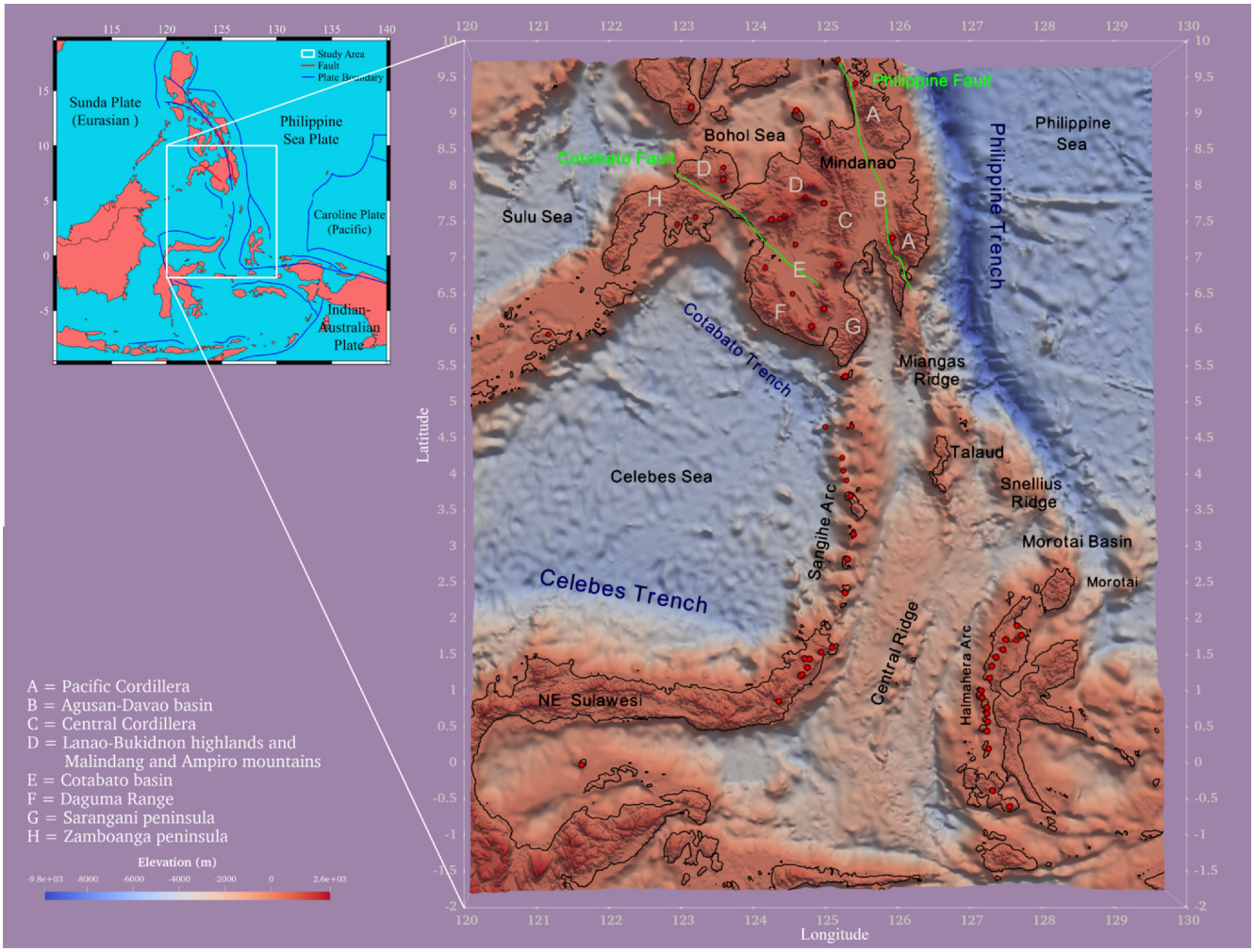

Fig. 1. Elevation (ETOPO1, Amante and Eakins, 2009) in the Mindanao-Molucca region with geographic and terrane names in the study labeled. Red triangles are volcanoes from the Smithsonian Institution Global Volcanism Program (Siebert and Simkin, 2002). Structures in Mindanao are modified from Sajona et al. (1994). Study area is shown by the rectangular box in the inset. (For interpretation of the references to colour in this figure legend, the reader is referred to the web version of this article.)

resolution 3D *P*-wave tomography of regional scale recently imaged the Philippine Sea slab along the southern Philippine Trench down to depths of 450–600 km with an apparently overturned dip angle, and the initiation of subduction was inferred at 20–25 Ma (Fan and Zhao, 2018).

In this study, we examine recently released global seismic datasets in 3D visualization to study slab configurations in the Mindanao-Molucca region. The EHB catalogue incorporates depth phases (pP, sP, pwP) at each iteration of hypocenter determination, thus avoiding trade-offs between depth and origin time (Engdahl et al., 1998). Recently released ISC-EHB data update the catalogue to cover the 1964–2016 period (Engdahl et al., 2019). With an ~50-year accumulation of well constrained earthquake hypocenters, more detailed 3D slab configurations can be imaged. Meanwhile, the Global CMT (GCMT) catalogue routinely inverted for centroid moment tensors of earthquakes (M_w > ~5) that are suitable for investigating the stress states of slabs through the **P**- and **T**-axes of earthquakes (Ekström et al., 2012). Based on EHB and GCMT locations and additional constraints, such as active-source seismic data, oceanic trenches, receiver functions, and seismic tomography models, Slab2 was recently issued to be a comprehensive model for global subduction zone geometries (Hayes et al., 2018).

2. Methods and datasets

We investigate patterns of seismic strain partitioning, which is an indication of current relative plate motions as taken up seismically, by plotting spatial distributions of earthquakes shallower than 60 km with their focal mechanisms. We separate the plot of thrust events from that of strike-slip and normal events, accompanying each with a corresponding plot showing the sizes of earthquakes by scaled sizes of circles (Figs. 3 and 4). Next, we visualize 3D configurations of slab material below 80 km depth, using the open-source, multi-platform data analysis package ParaView (Ayachit, 2015). By importing earthquake hypocenters from ISC-EHB (using all three levels of category) and subduction zone geometry from Slab2, we are able to adjust the perspective that is optimal for observing the slab configurations and to examine how well the Wadati-Benioff seismicity fits Slab2. Although ISC-EHB data constitute the main source for slab geometry determinations, the additional constraints – active-source seismic data, oceanic trenches, receiver functions, seismic tomography models – incorporated in Slab2 facilitate 3D modeling of slab structures in complex regions that are otherwise impossible to model using locations of earthquake alone (Hayes et al., 2018). For the complex arc-arc collision of the Mindanao-Molucca region, it is worthwhile not only to visualize the slab geometry but also to validate Slab2 with earthquake distributions from the ISC-EHB. We conduct the comparison for (1) the Molucca Sea slab, (2) the Philippine

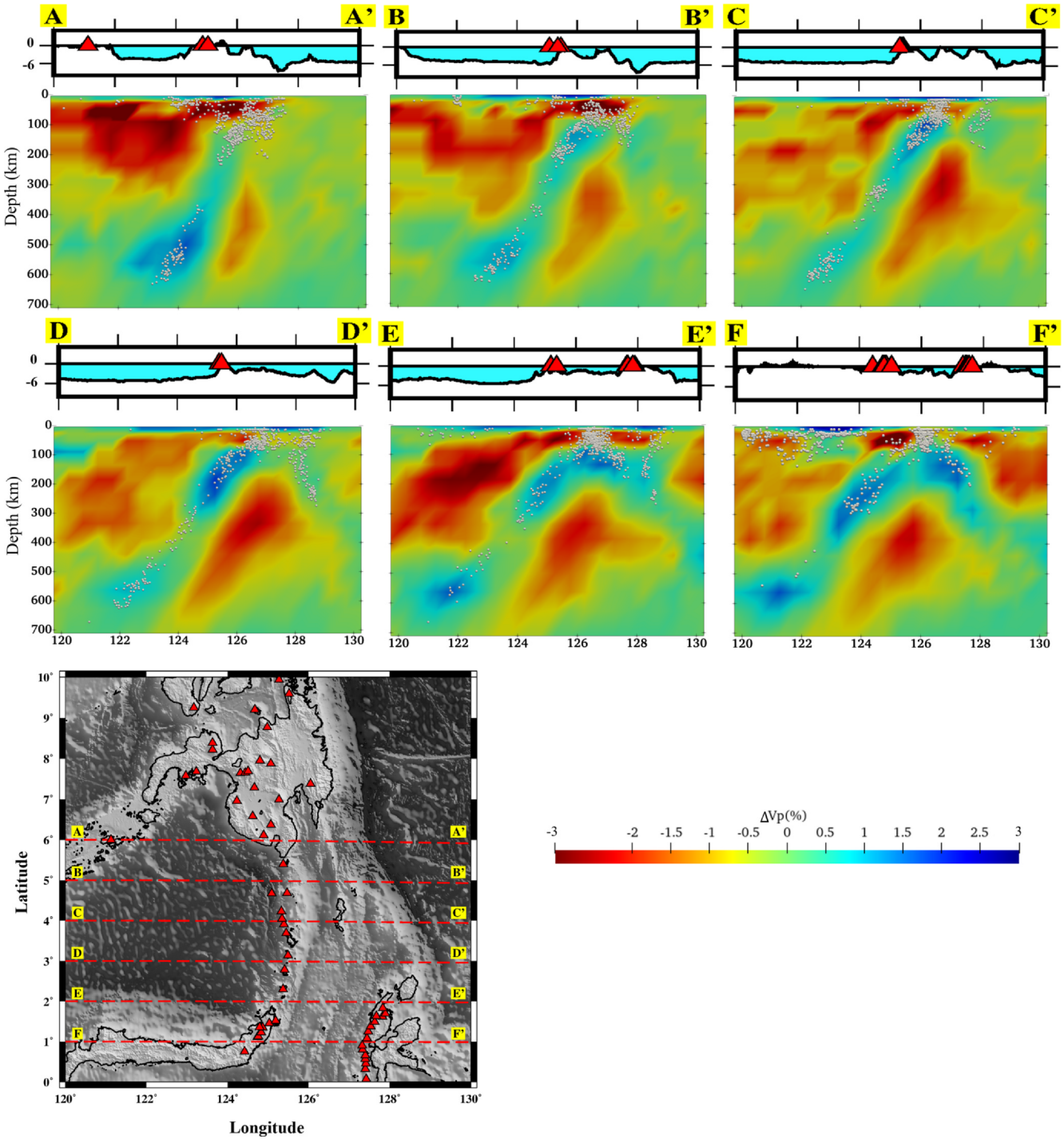

Fig. 2. East-west vertical cross-section of P-wave velocity anomalies obtained from UU-P07 global tomography model (Amaru, 2007). Locations of the six profiles are shown on the inset map, and scale bar denotes velocity perturbations. White dots and red triangles represent earthquakes and volcanoes, respectively, within a 50 km width on both sides of the profile. The upper panel on each profile indicates bathymetry. (For interpretation of the references to colour in this figure legend, the reader is referred to the web version of this article.)

Sea slab, and (3) the Molucca Sea and Philippine Sea plus Cotabato slabs, in sequence (Figs. 5–7). Finally, in order to better delineate the spatial variation of the east-dipping slab beneath the southern Philippine Trench, we group events into three boxes (A, B, C), based on visual examinations of seismicity patterns. Because of the complex seismicity distributions, the boxes are irregularly shaped and each employs a different projection method. Box A is projected with N65° azimuth. Seismicity (3–5°N) in Box B exhibits a slight curvature. Using earthquakes between 80 and 110 km depth, we first fit with an arc by polynomial regression (order 2) and fit the arc with a small circle centered at O (Fig. 8). The seismicity is then projected relative to O (Chen et al., 2004). For seismicity in Box C, we found that the projection with O results in a linear and compact slab and adopted it accordingly (Fig. 8). For the Halmahera slab, we fit the Halmahera Arc with a small circle and determine the center D. The ISC-EBH events (deeper than 80 km) in the area were grouped into Boxes D1 (excluding those of Box C) and D2 and projected with center D (Fig. 9). Finally, the GCMT deep earthquakes (deeper than 80 km) within each box (A, B, C,

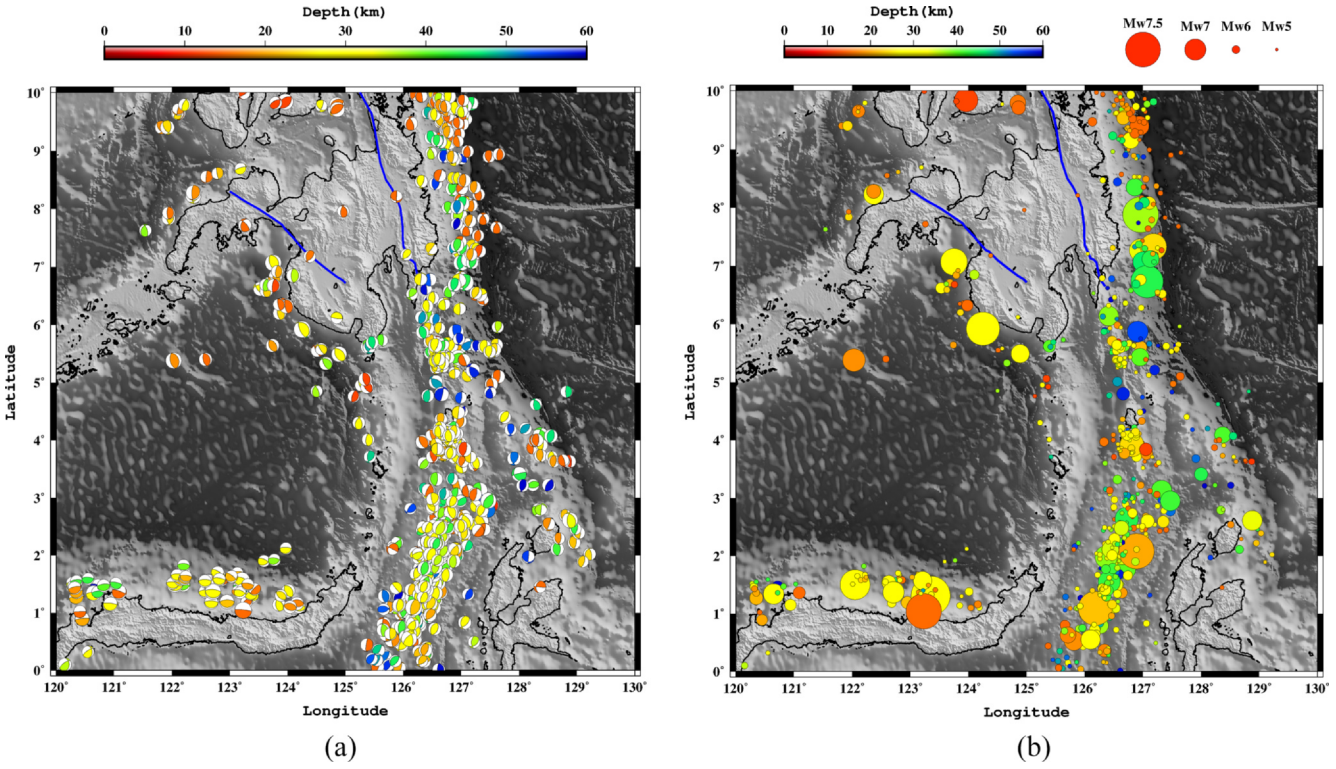

Fig. 3. (a) Distributions of thrust type earthquakes from the GCMT catalogue in the study area with depths color-keyed. (b) The size of earthquake is indicated by the size of the circle symbol. Notice the active areas in the Central Ridge, the segment of the Philippine Trench offshore Mindanao, the Cotabato Trench, and Talaud. (For interpretation of the references to colour in this figure legend, the reader is referred to the web version of this article.)

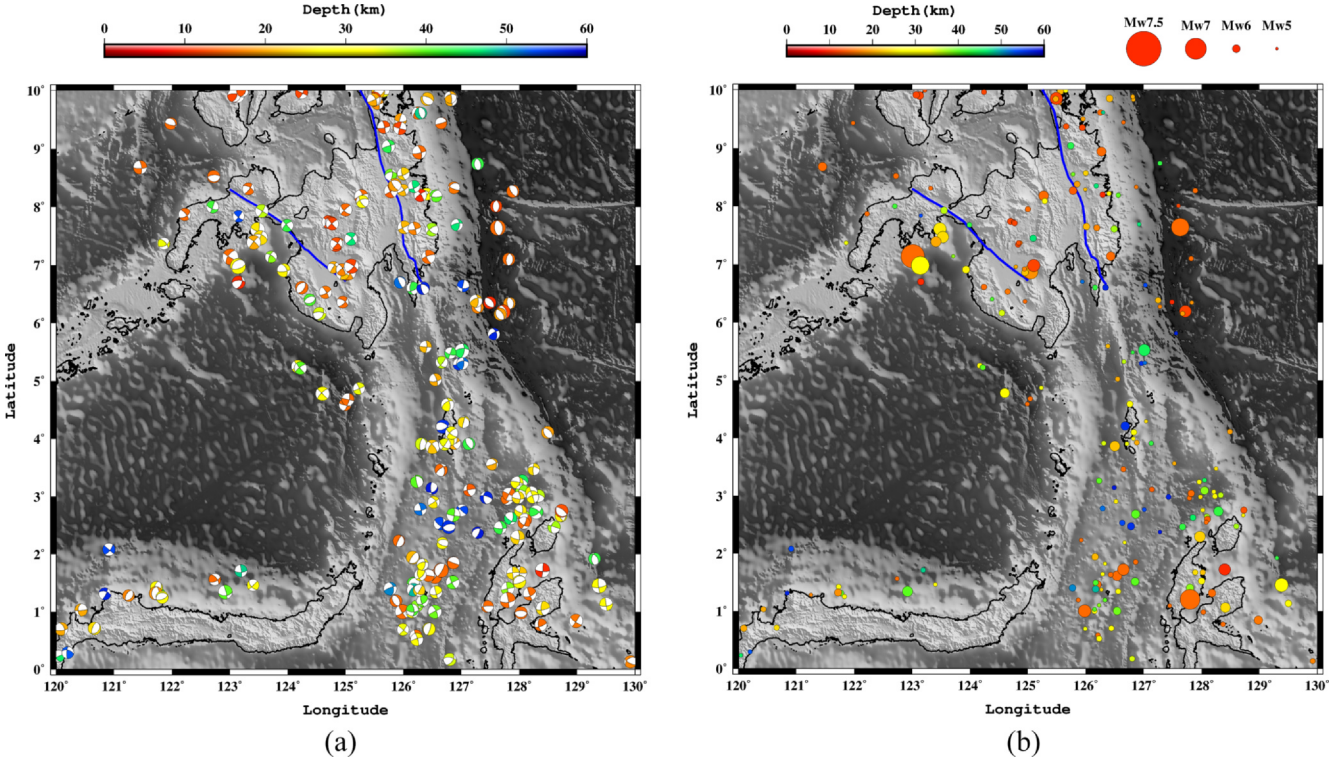

Fig. 4. (a) Distributions of strike-slip and normal types of earthquakes from the GCMT catalogue in the study area with depths color-keyed. (b) The size of earthquake is indicated by the size of the circle symbol. Notice the dominant strike-slip events in Mindanao and active areas in southern Halmahera and Morotai. (For interpretation of the references to colour in this figure legend, the reader is referred to the web version of this article.)

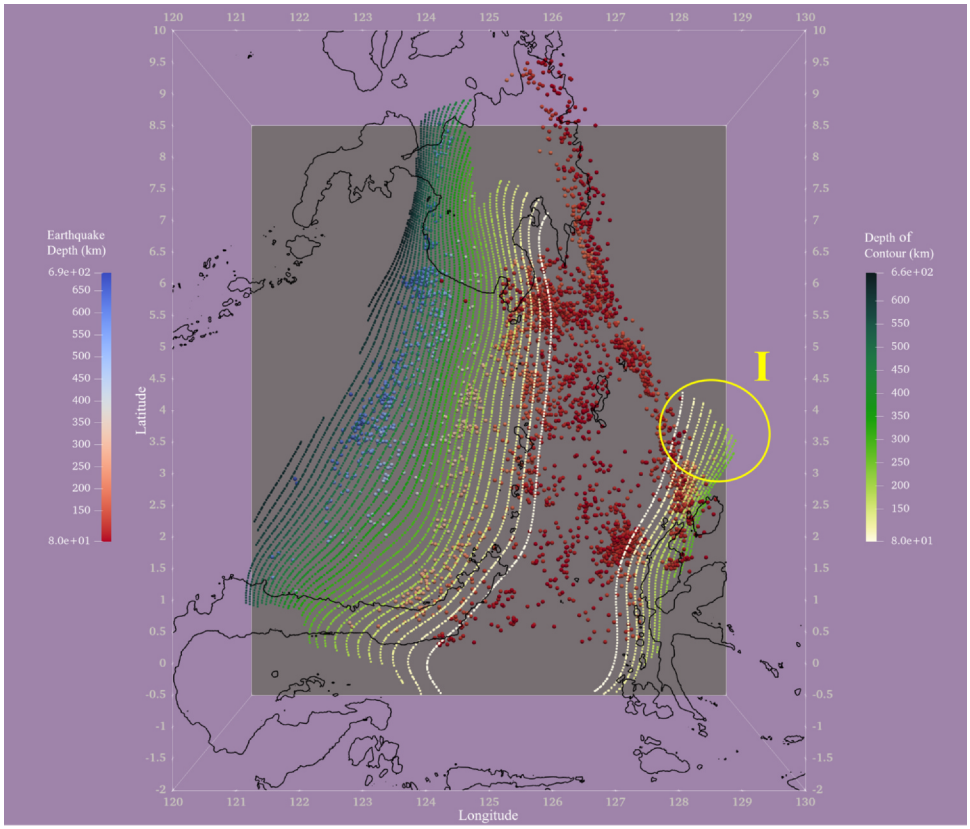

Fig. 5. (a) Map view of earthquake distribution from the ISC-EHB with depths greater than 80 km, and slab contours of the Molucca slab with depths greater than 80 km on a 20-km interval (Sangihe slab to the west and Halmahera slab to the east). The contour color bar is used for the Molucca slab here and in Fig. 7. Note how the deep portion (> ~150 km) of the Halmahera contours are not constrained by ISC-EHB earthquakes (circle marked by I). (b) Looking from a northward perspective with a slight dip angle. Circles marked by I and II indicate earthquakes above the contours that will be later modeled by contours of the Cotabato and Philippine slabs, respectively (Fig. 7). (For interpretation of the references to colour in this figure legend, the reader is referred to the web version of this article.)

D1, D2) were sorted out and their **P**- and **T**-axes projected with geographical coordinates (North-East-Down; Chen et al., 2001)(Fig. 10).

3. Results

Thrust-type earthquakes shallower than 60 km can be categorized into those induced by collision and those inter-plate events induced by subduction (Fig. 3). For the former, a linear distribution from the

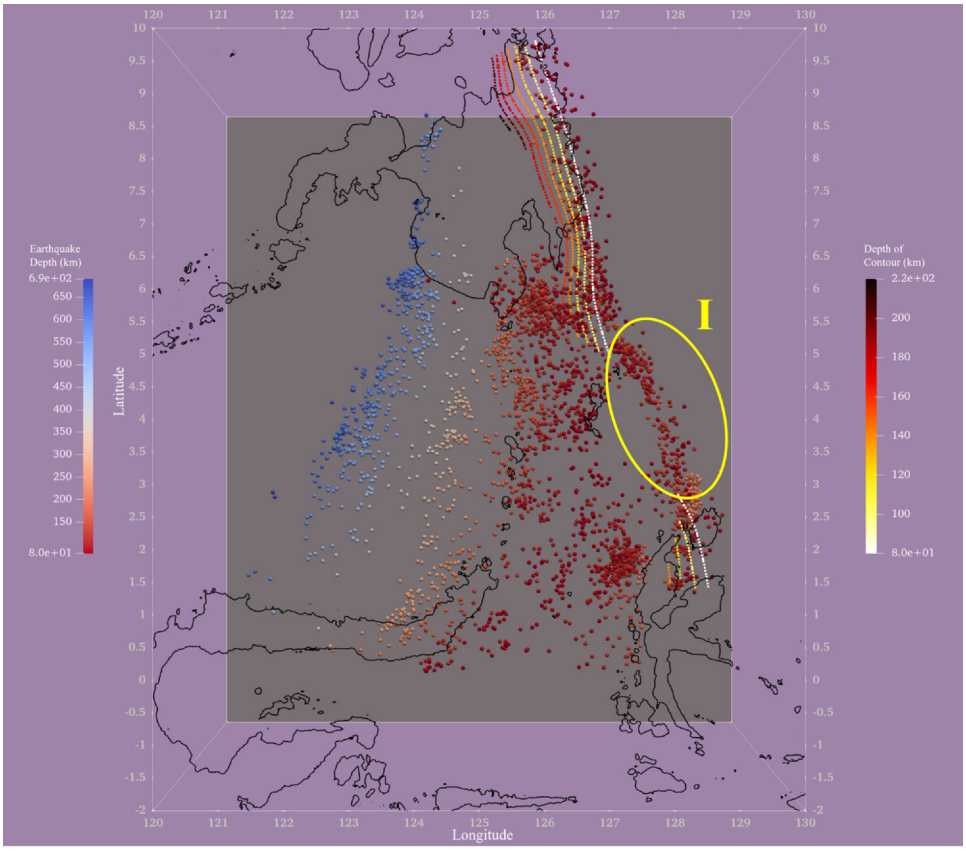

(a)

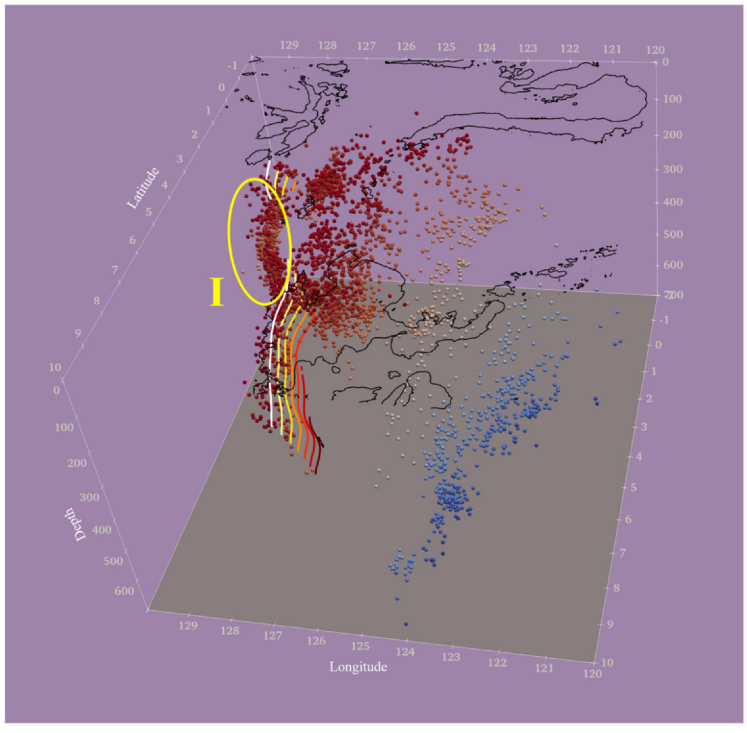

(b)

Fig. 6. (a) The same as Fig. 5(a) but for contours of the Philippine slab with depths greater than 80 km on a 20-km interval. The contour color bar is used for the Philippine and Cotabato slab here and in Fig. 7. (b) Looking from a nearly southward perspective with a slight dip angle. Note the ISC-EHB earthquakes marked by I representing an east-dipping zone that is not modeled by contours of the Philippine slab. (For interpretation of the references to colour in this figure legend, the reader is referred to the web version of this article.)

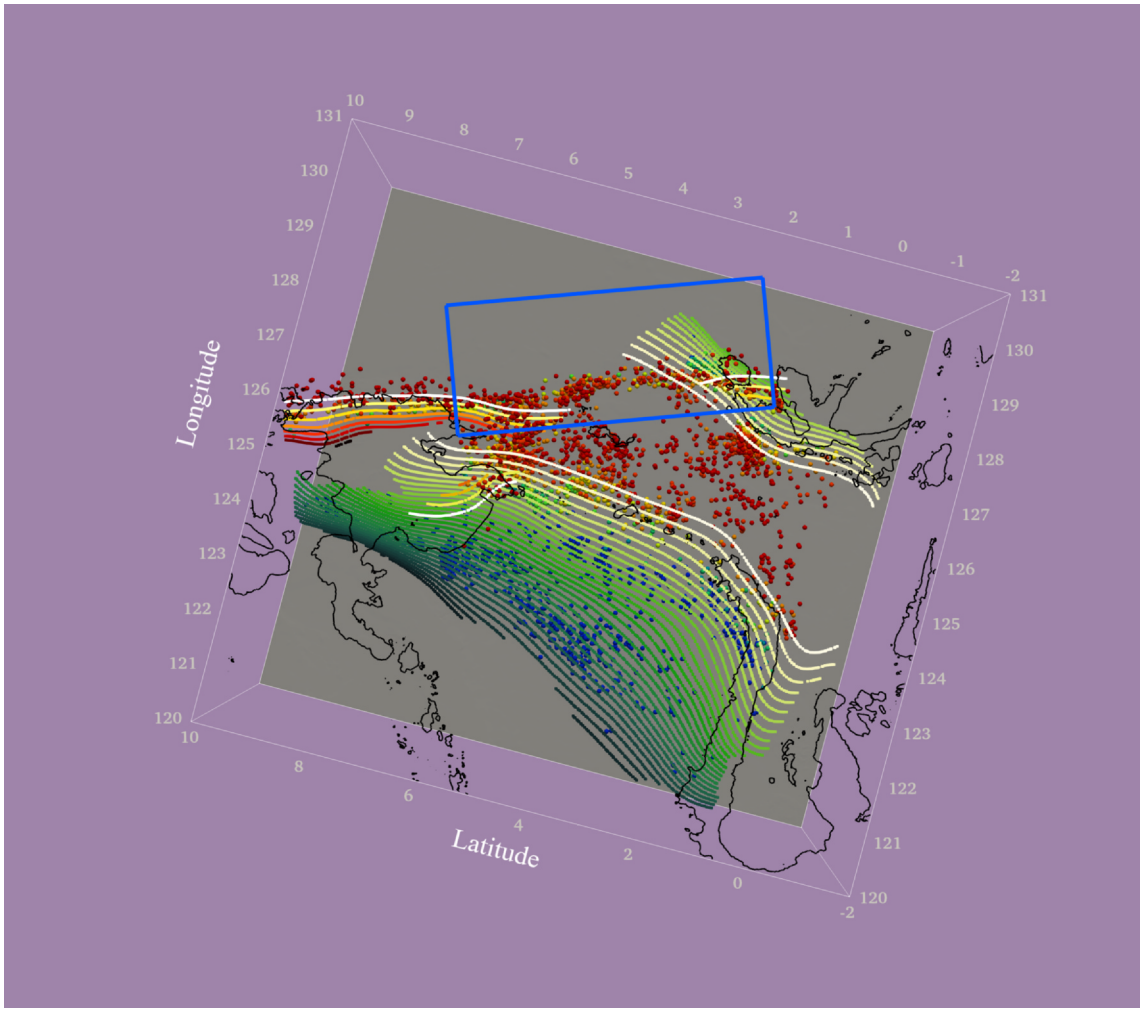

Fig. 7. Similar to Fig. 5(a) but with a ~60° counterclockwise rotation. Contours of the Molucca, Philippine, and Cotabato slabs are shown in the same fashion to demonstrate their spatial relationships. Note that the earthquakes in the box are not modeled by Slab2.

southern end of the Central Ridge northward to the Miangas Ridge is observed, with the strikes of the faults following the ridge trend. It is interesting to note that the seismic activity correlates well with ridge heights (e.g., Talaud; Fig. 3b), suggesting a ridge provenance. This linear distribution northward deviates from the trend of the Sangihe Arc and merges with that of the Halmahera Arc, suggesting that the northward propagation of collision is mostly taken up on the east branch of the Molucca slab (the Halmahera slab). However, the collision does not extend into the Pacific Cordillera on Mindanao. For the latter, the Eurasia-Philippine Sea plate convergence in Mindanao is taken up by inter-plate earthquakes whose fault strikes are parallel to the trench and which dip shallowly in the subduction direction (Fig. 3a). Both the Cotabato Trench and the Philippine Trench north of 6°N exhibit significant seismic moment release of inter-plate earthquakes up to 40 km depth (Fig. 3b), suggesting present-day active subduction here. On the other hand, subduction along the Philippine Trench south of 6°N is relatively inactive.

For normal-type earthquakes in the Mindanao-Molucca region, we note that those outer-rise earthquakes east of the Philippine Trench are significantly reduced south of 6°N. Together with lack of significant inter-plate earthquakes and shallowing of bathymetry (Lallemand et al., 1998), this suggests that this segment of trench is in an incipient stage of subduction. There are three moderate earthquakes located on Daguma Range SW Mindanao (Fig. 4a), where NW orientations of reactivated normal fault earthquakes were interpreted as back-arc extension behind the Cotabato Trench (Pubellier et al., 1991). However, these three events show NE orientations. The majority of shallow earthquakes (depth $<$ 20 km) on Mindanao exhibit a type of strike-slip mostly distributed along Agusan-Davao and the Cotabato Basin in a left-lateral sense on the Philippine Fault and Cotabato Fault, respectively, with some shallow events occurring diffusely in between (Fig. 4a). These strike-slip events suggest that the Eurasian-Philippine Sea plate convergence rates are starting to be taken up by strike-slip movements in Mindanao, but they are still less dominant than inter-plate events in the Philippine and Cotabato Trenches (Fig. 3b and 4b). There are a significant number of strike-skip earthquakes distributed along the Central to Miangas Ridge, in the Morotai Basin, and on northern Halmahera Island (Fig. 4a). How these events relate to the scenarios of northerly propagating collision remains to be investigated.

Next, we focus on earthquake hypocenters and slab contours deeper than 80 km, in order to visualize 3D configurations of slab material in the Mindanao-Molucca region. The west-dipping Molucca plate lithosphere (Sangihe slab) beneath the Sangihe Arc exhibits a substantial planar slab zone extending deeply to ~700 km depth and latitudinally from 0°N to 9°N (Fig. 5), as far as beneath offshore N Mindanao (Bohol Sea). We derive the average strike and dip as being ~190° and ~50°, respectively, adopting the method of Chen et al. (2004). The east-dipping Molucca plate lithosphere (Halmahera slab) beneath the Halmahera Arc exhibits convex curvature following the arc, with greater and deeper seismicity (no deeper than 300 km in general) toward the northern segment of the Halmahera Arc (Fig. 5). The average dip angle is about 45°. The west-dipping Philippine slab follows the Philippine

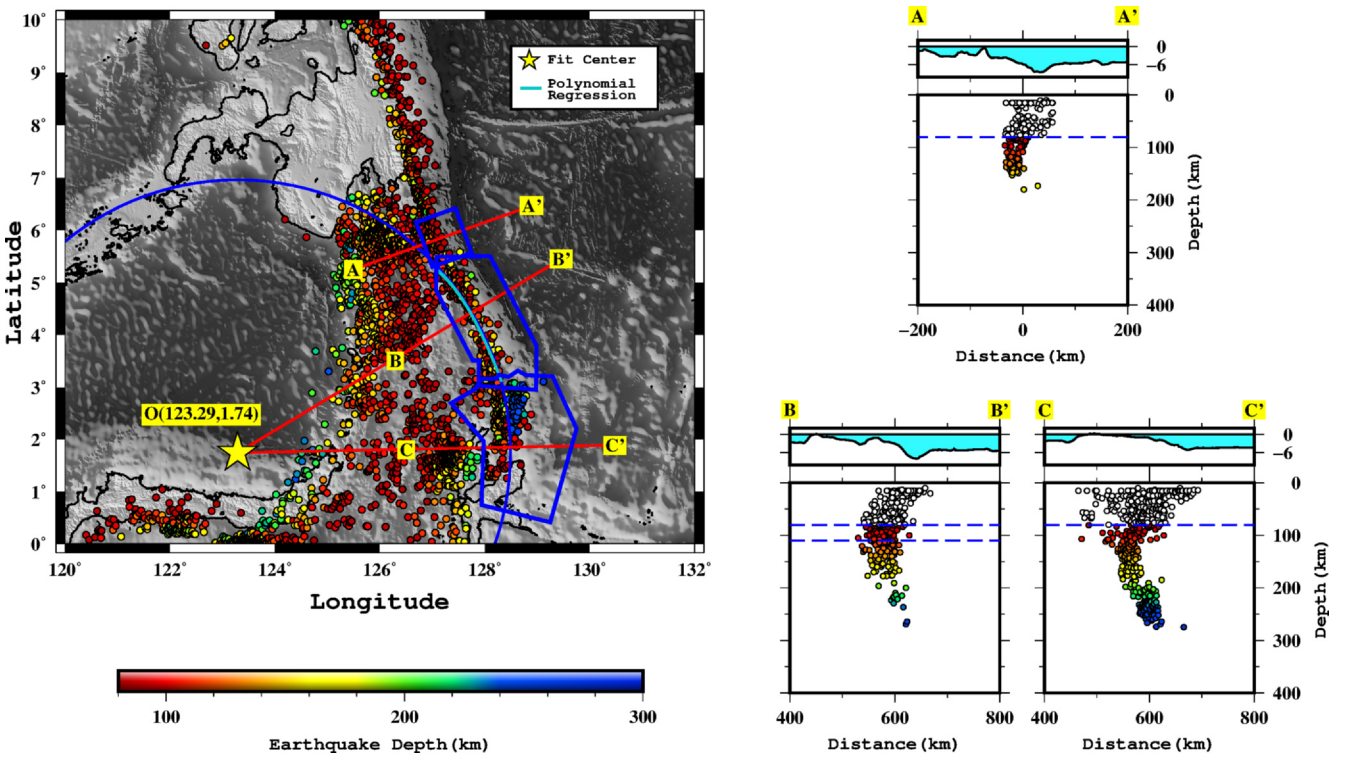

Fig. 8. (Left) Distributions of ISC-EHB earthquakes deeper than 80 km with shapes of grouping boxes A, B, C indicated. The center (O), with longitude and latitude indicated, of small circle is determined by fitting the cyan arc in Box B, which in turn is a result of 2nd-order polynomial regression using earthquakes between 80 and 110 km in Box B (double dashed lines in profile B). Those deeper than 240 km west of 126°E are not shown in the figure. (Right) Projection profiles of ISC-EHB earthquakes along the center of each box for the three boxes. Only those deeper than 80 km (dashed lines) are depth-color keyed. While Box A is projected on N65°E azimuth, Boxes B and C are projected using center O. (For interpretation of the references to colour in this figure legend, the reader is referred to the web version of this article.)

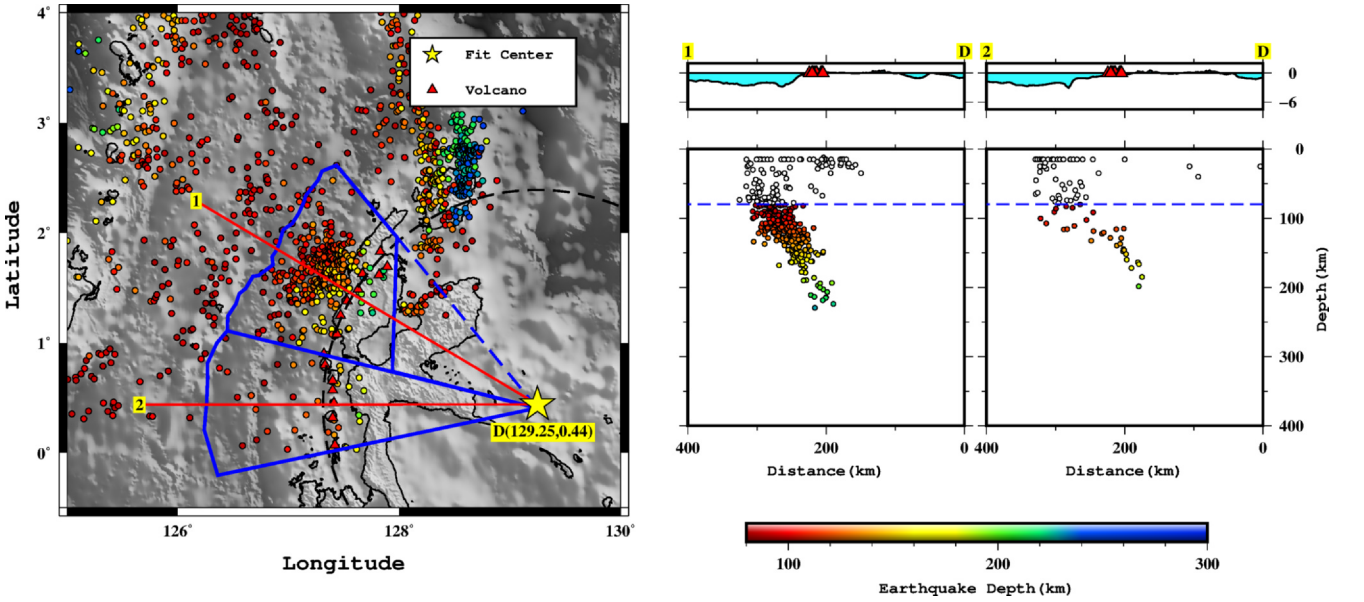

Fig. 9. Similar to Fig. 8 but for the Halmahera slab. Note that in D1 only those within the solid lines are included. Those in NE Halmahera are grouped into Box C and excluded from Box D1.

Trench, extending southward to ~5°N with depth no more than 200 km and average dip angle ~40°. According to Slab2, this west-dipping slab extends southerly to Morotai Island and East Halmahera (1°N), but contours greater than 80 km are missing in between (3°N–6°N) (Fig. 6). Adding contours of the Cotabato slab and assembling together all contours in the region (Fig. 7), those events above the Sangihe slab ~6°N are fit by the contours of the Cotabato slab and those beneath Morotai (2°N–3°N) exhibit a pattern with the west-dipping Philippine slab on top of the east-dipping Halmahera slab.

Upon projections of ISC-EHB events in Boxes A, B, and C, we observed that earthquakes greater than 80 km depth illuminate a steeply east-dipping slab between 1°N and 6°N (Fig. 8). For those in the

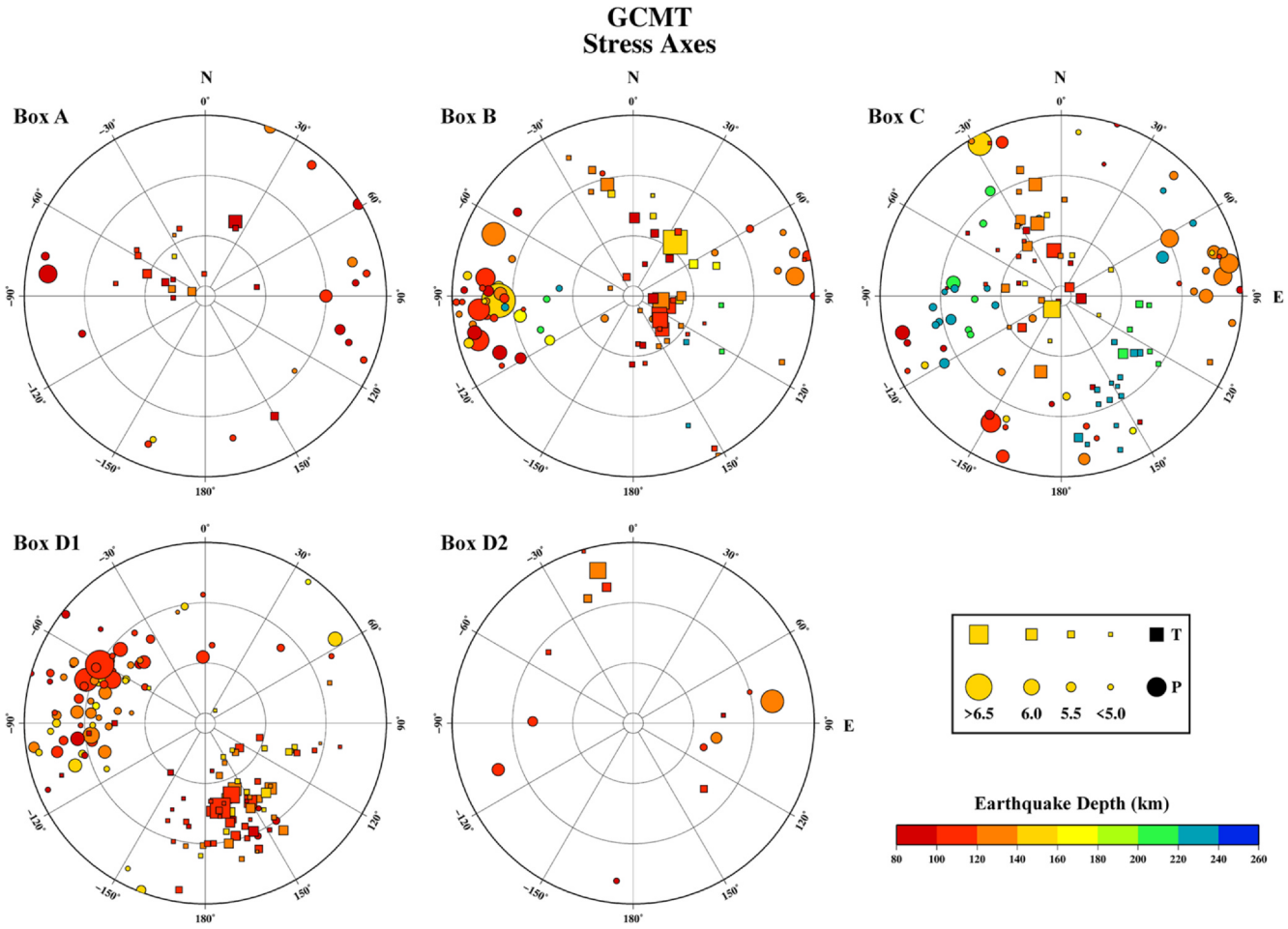

Fig. 10. Projection of **P**- and **T**-axes of GCMT earthquakes with depths deeper than 80 km within the five boxes in Figs. 8 and 9, using North-East-Down coordinates. Note that those shallower than 200 km in Boxes A, B, and C exhibit steeply plunging tension axes, that those greater than 200 km mostly occur in Box C with relatively small sizes exhibiting ~45° plunge with either SE **T**-axes or west **P**-axes, and that those in the Halmahera slab (Box D1) exhibit consistently down-dip extension.

Halmahera, we observed that seismicity patterns differ on the two sides of 128°E. To the left (N Halmahera), these are curved with the Halmahera Arc and are grouped into Box D1 (Fig. 9). To the right (NE Halmahera), these appear connected northerly with deep earthquakes beneath Morotai Island and are grouped into Box C (Fig. 8). Results of projected **P**- and **T**-axes for GCMT earthquakes greater than 80 km for Boxes A, B, C show three patterns - (1) down-dip extension for the majority of earthquakes between 80 and 200 km, (2) a few NNW azimuths with relatively shallowly plunging extension for earthquakes between 120 and 140 km, (3) in Box C, earthquakes greater than 200 km with relatively small size exhibiting SE azimuths with relatively shallowly plunging extension (Fig. 10). Those in the northern Halmahera slab (Box D1) show consistently SSE azimuth **T**-axes with around 45° plunge, in a down-dip extension pattern, while those in Box D2 are too few to be conclusively described (Fig. 10).

4. Discussion

Detailed analysis of spatial variations of ISC-EHB deep earthquakes (deeper than 80 km) between East Mindanao and Halmahera (Figs. 8 and 9) reveal a result that is not modeled by Slab2 – east-dipping seismicity between 3°N and 6°N (Boxes A and B) – along with another result that differs from Slab2 – east-dipping seismicity between 1°N and 3°N (Box C). For the latter, Slab2 treated seismicity of Box C as part of the present-day Halmahera slab and modelled them together with continuous contour lines. In this study, we separate them from earthquakes of the Halmahera slab (Fig. 8) and use the center (O), as inverted from events in Box B, for projection. Our treatment of deep earthquakes in Box C as a slab northerly continuous with those in Boxes B and A, instead of the Halmahera slab, can be justified by comparison with projections using center O and center D, respectively. Projection with center O clearly exhibits a more compact slab feature than projection with center D (Fig. S1).

To explain the nature of the east-dipping slab deeper than 80 km between 1°N and 6°N, we adopt the interpretation that the Snellius Ridge is the northern extension of the Halmahera Arc terrane (Moore and Silver, 1983) and the basement of east Mindanao is stratigraphically linked to the Halmahera Basement Complex (Hall, 1987). Accordingly, the east-dipping slab deeper than 80 km between 1°N and 6°N (Fig. 8) and the present-day Halmahera slab (Fig. 9) both belong to the east-dipping subduction of the Molucca Sea slab. The main difference is that the former represents deep relicts of earlier subduction, of which the shallow part (less than 80 km) has been significantly blurred by arc-arc collision of various degrees. Essentially, in a state of incipient collision, natural reduction of slab dip angle by process of slab rollback (trench retreat) must cease as buoyant continental or arc material approaches the trench. Slab dip angle then increases due to the negative thermal buoyancy of the slab, possibly enhanced by negative petrological buoyancy arising from equilibrium thermal uplift of the wadsleyite-forming “410-km” phase transition (Bina et al., 2020). Such slab steepening under the influence of such negative buoyancy forces induces an increasingly down-dip extensional stress regime within the

slab (Bina et al., 2020), and it also drives mantle return flow beneath the slab (Magni et al., 2012). These effects, together with consequent rheological weakening near the slab hinge, yield a period of trench advance (followed by subduction locking and ultimately succeeded by slab necking and detachment), and dynamical models generating such trench advance of order 100–200 km (Magni et al., 2012; Bina et al., 2020) seem consistent with the observed extent of trench dislocation in this region.

On the other hand, ISC-EHB earthquakes shallower than 80 km between 1°N and 6°N exhibit west-dipping slab traceable upward to the Philippine Trench (Fig. 8) and comply with the Slab2 model of the Philippine slab (Fig. 6). Given that the Philippine Trench here was a newly developed feature (Lallemand et al., 1998; Pubellier et al., 1999), we deem the changing polarity of dip angle near 100 km depth to be a present-day example of flipping subduction polarity (Su et al., 2019). While the east-dipping Molucca slab ceased subduction due to arc-arc collision, the west-dipping Philippine slab initiated subduction to accommodate regional Eurasian-Philippine Sea relative motions. Because polarity flipping occurred only since the Late Tertiary, the relict Molucca slab still retains its cold temperatures and apparently dehydrates to produce east-dipping intermediate-depth earthquakes. The intertwined earthquakes from subduction of opposing polarities also hindered the assessments of earlier studies, using data available ~40 years ago, by which Cardwell et al. (1980) inferred the absence of east-dipping slab north of 3°N and McCaffrey (1982) identified an east-dipping slab separated from the Halmahera slab but ending at about 3.5°N.

The explanation of the steeply east-dipping slab between 1°N and 6°N (Fig. 8), with the majority of earthquakes between 80 and 200 km exhibiting predominantly steeply plunging **T**-axes (Fig. 10), is analogously consistent with observations (Chen et al., 2015, 2020) and models (Bina et al., 2020) of the present-day arc-continent collision in NW Mindoro at the southern end of the Manila Trench. However, the explanation is contradictory with the suggestion of Fan and Zhao (2018) that the entire Wadati-Benioff zone belongs to the Philippine slab with an apparently overturned dip angle and that subduction in the Philippine Trench south of 6°N initiated at 20–25 Ma. In geodynamic models, an overturned dip of the slab is only observed under special circumstances, typically involving viscous coupling of the slab tip with the top of the lower mantle (Čížková and Bina, 2015). Here, however, the suggested overturn at a depth of ~100 km disallows interaction with the 660-km discontinuity to generate bending stresses for overturn. Although the dynamics of double slab subduction (Holt et al., 2017) was invoked by Fan and Zhao (2018) as a potential mechanism for slab overturn, how the subducting Sangihe slab and Philippine Sea slab correspond to the model remains to be established.

There are some aspects of observation not well explained by our flipping subduction polarity hypothesis as well. (1) Small earthquakes deeper than 200 km in Box C deviate from steeply plunging **T**-axes (Fig. 10). One speculative explanation is that the depth-extent of the slab is increasing from N to S, resulting a more negative buoyant slab in the S than in the N. (2) The spatial relationship between seismicity (greater than 80 km) in N Halmahera (Box D1) and that in NE Halmahera (Box C) is also intriguing. GCMT earthquakes shallower than 60 km offshore NW Morotai Island exhibiting consistently NW-striking nodal planes with right-lateral strike-slip may partly explain the offset. As a final remark, orientations of **B**-axes (Fig. S3) reveal that a simple 2-D geodynamic model is reasonably applicable for Boxes A and B by their largely horizontal ~NS **B**-axes (Bina et al., 2020). On the other hand, the pattern becomes more complicated in Box C, suggesting a more 3-D set of driving forces is becoming significant, which may relate to the apparent transition of the arc from roughly linear to clearly curved.

5. Conclusions

Recently released seismic datasets and 3D visualization techniques together allow us to analyze the northerly transition from arc-arc collision to flipping subduction polarity along the Philippine Trench. For earthquakes shallower than 60 km, distributions of thrust-type GCMT events suggest present-day collision mostly occurs along the Central Ridge and Talaud-Miangas Ridge. At Mindanao, while inter-plate earthquakes are large and abundant in the Philippine Trench, earthquakes on the island are dominantly of strike-slip type. For earthquakes deeper than 80 km, we identify a steeply east-dipping zone beneath the southern end of the Philippine Trench (1°N–6°N), where those shallower than 200 km exhibit dominantly steeply plunging **T**-axes, consistent with the characteristics of a slab upon incipient collision. The west-dipping Philippine slab above it presents a present-day example of flipping subduction polarity.

CRediT authorship contribution statement

Po-Fei Chen: Conceptualization, Methodology, Formal analysis, Investigation, Writing - original draft, Project administration, Funding acquisition. **Mei Chien:** Software, Visualization. **Craig R. Bina:** Conceptualization, Writing - review & editing. **Hung-Yu Yen:** Investigation. **Erlinton A. Olavere:** Data curation.

Declaration of Competing Interest

The authors declare that they have no known competing financial interests or personal relationships that could have appeared to influence the work reported in this paper.

Acknowledgements

We thank Prof. E. Robert Engdahl and one anonymous reviewer for constructive comments. This work was supported by the Taiwan Earthquake Research Center (TEC) funded through the Ministry of Science and Technology (MOST) of Taiwan with Grant Number 108-2116-M-008-009 and by the Central Weather Bureau with Grant Number MOTC-CWB-109-E-05. The TEC contribution number for this article is 00164. Some figures were prepared with the Generic Mapping Tools (Wessel and Smith, 1998).

Appendix A. Supplementary data

Supplementary data to this article can be found online at https://doi.org/10.1016/j.jaesx.2020.100034.

References

Amante, C., Eakins, B.W., 2009. ETOPO1 1 Arc-Minute Global Relief Model: Procedures, Data Sources and Analysis. NOAA Technical Memorandum NESDIS NGDC-24. National Geophysical Data Center, NOAA.

Amaru, M.L., 2007. Global travel time tomography with 3-D reference models. Utrecht University (PhD Thesis).

Ayachit, U., 2015. The ParaView guide: A Parallel Visualization Application. 303 Kitware, Clifton Park, NY.

Bina, C.R., Čížková, H., Chen, P.-F., 2020. Evolution of subduction dip angles and seismic stress patterns during arc-continent collision: modeling Mindoro Island. Earth Planet. Sci. Lett. 533, 116054.

Čížková, H., Bina, C.R., 2015. Geodynamics of trench advance: insights from a Philippine-Sea-style geometry. Earth Planet. Sci. Lett. 430, 408–415.

Cardwell, R.K., Isacks, B.L., Karig, D.E., 1980. The spatial distribution of earthquakes: focal mechanism solutions and subducted lithosphere in the Philippine and northeastern Indonesian islands. In: Hayes, D.E. (Ed.), The Tectonic and Geologic Evolution of Southeast Asian Seas and Islands. Am. Geophys. Union Monogr., vol. 23, pp. 1-35.

Chen, P.-F., Bina, C.R., Okal, E.A., 2001. Variations in slab dip along the subducting Nazca Plate, as related to stress patterns and moment release of intermediate-depth seismicity and to surface volcanism. Geochem. Geosyst. 2. https://doi.org/10.1029/2001GC000153.

Chen, P.-F., Bina, C.R., Okal, E.A., 2004. A global survey of stress orientations in subducting slabs as revealed by intermediate-depth earthquakes. Geophys. J. Int. 159, 721–733.

Chen, P.-F., Olavere, E.A., Wang, C.-W., Bautista, B.C., Solidum Jr., R.U., Liang, W.-T.,

2015. Seismotectonics of Mindoro, Philippines. Tectonophysics 640–641, 70–79.
Chen, P.-F., Su, P.-L., Olavere, E.A., Solidum Jr., R.U., Hunag, B.-S., 2020. Relocation of the April 2017 Batangas, Philippines, earthquake sequence, with tectonic implications. Terr. Atmos. Ocean. Sci. 31, 1–10. https://doi.org/10.3319/TAO.2020.01.31.01.
Ekström, G., Nettles, M., Dziewoński, A.M., 2012. The global CMT project 2004–2010: Centroid-moment tensors for 13,017 earthquakes. Phys. Earth Planet. Inter. 200–201, 1–9.
Engdahl, E.R., Di Giacomo, D., Sakarya, B., Gkarlaouni, C.G., Harris, J., Storchak, D.A., 2019. ISC-EHB 1964–2016, an Improved Data Set for Studies of Earth Structure and Global Seismicity. Earth and Space Science 7, e2019EA000897. https://doi.org/10.1029/2019EA000897.
Engdahl, E.R., Van Der Hilst, R.D., Buland, R.P., 1998. Global teleseismic earthquake relocation with improved travel times and procedures for depth determination. Bull. Seismol. Soc. Am. 88, 722–743.
Fan, J., Zhao, D., 2018. Evolution of the southern segment of the Philippine Trench: Constraints from seismic tomography. Geochem. Geophys. Geosyst. 19, 4612–4627.
Hall, R., 1987. Plate boundary evolution in the Halmahera region, Indonesia. Tectonophysics 144, 337–352.
Hall, R., Spakman, W., 2015. Mantle structure and tectonic history of SE Asia. Tectonophysics 658, 14–45.
Hayes, G.P., Moore, G.L., Portner, D.E., Hearne, M., Flamme, H., Furtney, M., Smoczyk, G.M., 2018. Slab2, a comprehensive subduction zone geometry model. Science 362, 58–61.
Holt, A.F., Royden, L.H., Becker, T.W., 2017. The dynamics of double slab subduction. Geophys. J. Int. 209, 250–265.
Lallemand, S.E., Popoff, M., Cadet, J.-P., Bader, A.-G., Pubellier, M., Rangin, C., Deffontaines, B., 1998. Genetic relations between the central and southern Philippine Trench and the Sangihe Trench. J. Geophys. Res. Solid Earth 103, 933–950.
Magni, V., van Hunen, J., Funiciello, F., Faccenna, C., 2012. Numerical models of trench migration in continental collision zones. Solid Earth Discuss. 4, 429–458.
McCaffrey, R., 1982. Lithospheric deformation within the Molucca Sea arc-arc collision: Evidence from shallow and intermediate earthquake activity. J. Geophys. Res. 87, 3663–3678.
Moore, G.F., Silver, E.A., 1983. Collision processes in the northern Molucca Sea. In: Hayes, D.E. (Ed.), The Tectonic and Geologic Evolution of Southeast Asian Seas and Islands. American Geophysical Union, Geophysical Monograph, vol. 27, pp. 360-372.
Nichols, G., Hall, R., Milsom, J., Masson, D., Parson, L., Sikumbang, N., Dwiyanto, B., Kallagher, H., 1988. The southern termination of the Philippine Trench Tectonophysic. Elsevier Science Publishers B.V., Amsterdam 304, pp. 289-303.
Pubellier, M., Quebral, R., Rangin, C., Deffontaines, B., Muller, C., Butterlin, J., Manzano, J., 1991. The Mindanao, collision zone, a soft collision event within a continuous strike-slip setting. J. SE Asian Earth Sci. 6, 239–248.
Pubellier, M., Bader, A.G., Rangin, C., Deffontaines, B., Quebral, R., 1999. Upper plate deformation induced by subduction of a volcanic arc: the Snellius Plateau (Molucca Sea, Indonesia and Mindanao, Philippines). Tectonophysics 304, 345–368.
Quebral, R.D., Pubellier, M., Rangin, C., 1996. The onset of movement on the Philippine Fault in eastern Mindanao: a transition from a collision to a strike-slip environment. Tectonics 15, 713–726.
Sajona, F.G., Bellon, H., Maury, R.C., Pubellier, M., Cotten, J., Rangin, C., 1994. Magmatic response to abrupt changes in geodynamic settings: Pliocene—Quaternary calc-alkaline and Nb-enriched lavas from Mindanao (Philippines). Tectonophysics 237, 47–72.
Seno, T., Stein, S., Gripp, A.E., 1993. A model for the motion of the Philippine Sea plate consistent with NUVEL-1 and geological data. J. Geophys. Res. 98, 17941–17948.
Siebert, L., Simkin, T., 2002. Volcanoes of the World: an Illustrated Catalog of Holocene. Volcanoes and their Eruptions. Smithsonian Institution, Global Volcanism Program. Digital Information Series, GVP-3.
Soesoo, A., Bons, P.D., Gray, D.R., Foster, D.A., 1997. Divergent double subduction: tectonic and petrologic consequences. Geology 8, 755–758.
Su, P.L., Chen, P.F., Wang, C.Y., 2019. High-resolution 3-D P wave velocity structures under NE Taiwan and their tectonic implications. J. Geophys. Res. Solid Earth 124, 601–614.
Wessel, P., Smith, W.H.F., 1998. New, improved version of the Generic Mapping Tools Released. Eos. Trans. Am. Geophys. Union 79, 579.